

Gas/particle partitioning of carbonyls in the photooxidation of isoprene and 1,3,5-trimethylbenzene

R. M. Healy¹, J. C. Wenger¹, A. Metzger², J. Duplissy², M. Kalberer^{2,3}, and J. Dommen³

¹Department of Chemistry and Environmental Research Institute, University College Cork, Cork, Ireland

²Laboratory of Atmospheric Chemistry, Paul Scherrer Institut, Villigen, Switzerland

³Department of Chemistry and Applied Biosciences, ETH Zurich, 8093 Zurich, Switzerland

Received: 11 January 2008 – Accepted: 11 January 2008 – Published: 5 March 2008

Correspondence to: J. C. Wenger (j.wenger@ucc.ie)

Published by Copernicus Publications on behalf of the European Geosciences Union.

4727

Abstract

A new denuder-filter sampling technique has been used to investigate the gas/particle partitioning behaviour of the carbonyl products from the photooxidation of isoprene and 1,3,5-trimethylbenzene. A series of experiments was performed in two atmospheric simulation chambers at atmospheric pressure and ambient temperature in the presence of NO_x and at a relative humidity of approximately 50%. The denuder and filter were both coated with the derivatizing agent O-(2,3,4,5,6-pentafluorobenzyl)-hydroxylamine (PFBHA) to enable the efficient collection of gas- and particle-phase carbonyls respectively. The tubes and filters were extracted and carbonyls identified as their oxime derivatives by GC-MS. The carbonyl products identified in the experiments accounted for around 5% and 10% of the mass of secondary organic aerosol formed from the photooxidation of isoprene and 1,3,5-trimethylbenzene respectively.

Experimental gas/particle partitioning coefficients were determined for a wide range of carbonyl products formed from the photooxidation of isoprene and 1,3,5-trimethylbenzene and compared with the theoretical values based on standard absorptive partitioning theory. Photooxidation products with a single carbonyl moiety were not observed in the particle phase, but dicarbonyls, and in particular, glyoxal and methylglyoxal, exhibited gas/particle partitioning coefficients several orders of magnitude higher than expected theoretically. These findings support the importance of heterogeneous chemistry as a pathway for SOA formation and growth during the atmospheric degradation of anthropogenic and biogenic hydrocarbons.

1 Introduction

The atmospheric degradation of volatile organic compounds (VOCs) yields a range of oxygenated products that, depending on their physical and chemical properties, can lead to the formation of secondary organic aerosol (SOA). There is considerable interest in SOA because it accounts for a significant fraction (up to 80%) of ambient at-

4728

mospheric aerosol and can therefore affect climate and human health (Pöschl, 2005). Despite extensive efforts over recent years, there remain uncertainties in the environmental impact of SOA, because of a lack of knowledge on the sources, composition, properties and mechanisms for its formation (Fuzzi et al., 2006).

5 Biogenic and anthropogenic sources of VOCs both contribute to SOA formation. Until very recently the major biogenic SOA precursors were believed to be the terpenes and sesquiterpenes. However, the importance of isoprene as a biogenic SOA precursor has been confirmed in a number of recent field and laboratory experiments (Claeys et al., 2004; Dommen et al., 2006; Edney et al., 2005; Kleindienst et al., 2006; Kroll
10 et al., 2005, 2006). Whilst biogenic VOCs are the dominant contributors to global SOA formation, anthropogenic species such as the aromatic compounds (benzene, toluene, xylenes and trimethylbenzenes) can contribute significantly to the production of SOA in urban areas (Kanakidou et al., 2005). A considerable amount of information on the SOA-forming potential of individual biogenic and anthropogenic VOCs has
15 been obtained from simulation chamber experiments performed over the last 10 years (Kroll et al., 2006; Ng et al., 2007; Odum et al., 1997). However, elucidation of the processes and chemical species responsible for SOA formation has proven more difficult. Although a number of recent studies have utilised state-of-the-art methods to investigate the chemical composition of SOA, in general the overall yield of products
20 detected in the particle phase is typically less than 30% (Forstner et al., 1997; Hamilton et al., 2005). Some of the species detected in SOA are first generation oxidation products that have partitioned into the particle phase, while others are formed through further gas-phase oxidation of the products followed by partitioning (Jang and Kamens, 2001). In addition, the identification of oligomers in SOA has added further complexity
25 to the overall mechanistic picture of SOA formation and indicates that heterogeneous and particle-phase reactions may also play an important role (Dommen et al., 2006; Kalberer et al., 2004).

Clearly more information is required to improve our understanding of SOA formation. An important piece of information that is often missing from chamber experiments is

4729

knowledge of the gas/particle partitioning of the VOC oxidation products, which can be particularly useful in determining the specific oxidation products involved in SOA formation. However, experimentally determined gas/particle partitioning coefficients of oxidation products have only been reported for a limited number of biogenic SOA pre-
5 cursors, such as α -pinene and other monoterpenes (Yu et al., 1999), and toluene as the only anthropogenic SOA precursor (Jang and Kamens, 2001). The objective of this work was to use a recently developed denuder-filter system (Temime et al., 2007) to investigate the gas/particle partitioning of the carbonyl photooxidation products of isoprene and 1,3,5-trimethylbenzene (1,3,5-TMB). Experiments were carried out in
10 simulation chambers at the Paul Scherrer Institut (PSI) and University College Cork (UCC) for intercomparison purposes. The results are used to determine experimental gas/particle partitioning coefficients and to provide insights into the oxidation products involved in SOA formation, along with their contribution to the chemical composition of the particle phase.

15 **2 Experimental**

2.1 PSI experiments

The simulation chamber at PSI has been used for several photooxidation studies and is described in detail elsewhere (Paulsen et al., 2005). Briefly, the apparatus consists of a cubic 27 m³ FEP Teflon foil chamber housed in a wooden temperature-controlled
20 enclosure. The walls and ceiling of the enclosure are covered with aluminium foil to maximize light intensity and diffusion. Light is provided by four xenon arc lamps (4 kW, XPO 4000 W/HS, OSRAM), with one in each corner of the enclosure. Borosilicate filters are located in front of each lamp to reduce actinic UV radiation below 300 nm.

Five photooxidation experiments were performed in the PSI chamber. The initial
25 starting conditions for the experiments are given in Table 1. All experiments were carried out at a relative humidity of approximately 50%, a temperature of 20°C, and

4730

atmospheric pressure. For each experiment the chamber was first humidified, followed by the introduction of NO and NO₂. Finally, known amounts of either isoprene or 1,3,5-TMB were evaporated in a heated glass bulb and introduced in a flow of purified air. The mixture was allowed to mix for 30 min before turning on the lights. Parent hydrocarbons and photooxidation products were monitored using proton-transfer mass spectrometry (PTR-MS) (Ionicon Analytik GmbH). Ozone was measured using a commercial Environics S300 instrument, whilst NO and NO₂ were quantified using a Thermo Environmental Instruments (42C) analyzer equipped with a photolytic converter to selectively reduce NO₂ to NO. Particle size distributions (14–964 nm in diameter) were measured with a scanning mobility particle sizer and a TSI 3010 condensation particle counter.

The gas- and particle-phase carbonyl oxidation products generated in the photooxidation experiments were separated and simultaneously collected using a denuder-filter sampling device recently developed at UCC (Temime et al., 2007). It consists of an annular denuder coated with XAD-4 resin and the derivatizing agent O-(2,3,4,5,6-pentafluorobenzyl)-hydroxylamine (PFBHA) to enable on-tube conversion of gas-phase carbonyls to their oxime derivatives which can be extracted and identified by GC-MS. The filter is also doped with PFBHA to enable collection of carbonyls in the particle phase. A second denuder tube is located downstream of the filter to trap any particle phase species that might revert to the gas phase during sampling. A schematic diagram of this denuder-filter-denuder (D-F-D) configuration is shown in Fig. 1.

The concentrations of the carbonyls produced in these photooxidation experiments were considerably smaller than those used in the original tests of the denuder performance (Temime et al., 2007). As a result, the amount of PFBHA used for coating the denuder tubes was reduced by a factor of four (to 0.02 g), while the filters were doped with 0.002 g of PFBHA. The use of a lower amount of PFBHA prompted another series of tests to ensure efficient collection of the gas-phase carbonyls. In order to determine the collection efficiency, an alternative sampling configuration, consisting of a filter-denuder-denuder (F-D-D), was employed as shown in Fig. 1. A second method to test the collection efficiency of the denuder was also performed. This involved placing

4731

the PTR-MS inlet at the entrance and exit of a coated denuder tube while the reaction mixture from the chamber was pumped through the denuder at 10 L min⁻¹. Thus the breakthrough of gas-phase products was measured in real time and an optimum sampling duration was evaluated.

The denuder-filter apparatus was located inside the temperature-controlled chamber housing in order to avoid a temperature gradient during sampling which could affect gas/particle partitioning of the photooxidation products. Based on the collection efficiency results a sampling duration of 50 min was chosen with a flow of 10 L min⁻¹. Denuder-filter samples were taken at regular intervals during each experiment using both the D-F-D and F-D-D configurations. The denuder tubes and filters were coated as described previously (Temime et al., 2007) and extracted immediately after sampling using a solvent mixture (methanol/dichloromethane/acetonitrile 0.5/8.5/1 v/v/v) (20 mL per tube and 10 mL per filter). The extracts were stored in the dark at room temperature overnight and then reduced to a known volume (approximately one third of the original volume) by rotary evaporation, filtered using a PTFE membrane filter (pore size 0.45 μm), transferred to vials and shipped to UCC for GC-MS analysis. Blank denuder and filter samples were prepared and extracted in the same way.

2.2 UCC experiments

Photooxidation of isoprene and 1,3,5-TMB was also performed in the simulation chamber at UCC in order to compare aerosol yields and partitioning data for the oxidation products formed in the two chambers. The UCC chamber is described in detail elsewhere (Temime et al., 2007). Briefly, the chamber is rectangular, made of FEP Teflon foil, has a volume of ca. 6500 L and is surrounded by 12 Philips TL12 (40 W) lamps with an emission maximum at 310 nm and 12 Philips TL05 (40 W) lamps with an emission maximum at 360 nm.

Four photooxidation experiments were performed in the UCC chamber. A summary of the initial conditions for the experiments is given in Table 1. The relative humidity was approximately 50% in each case. The chamber was humidified by flowing purified

4732

air through the headspace of an impinger containing heated Milli-Q water. Isoprene and 1,3,5-TMB were also introduced through a heated impinger and concentrations were monitored by GC-FID. NO and NO_x concentrations were measured with a chemiluminescence NO_x analyzer (Thermo Model 42i) and ozone was measured with a UV photometric O₃ analyzer (Thermo Model 49i). The formation and evolution of particles in the range 10–470 nm was monitored using a scanning mobility particle sizer (SMPS, TSI Model 3034).

Denuder-filter sampling in the UCC experiments was performed in the same manner as outlined above but with the sampling time reduced to 20 min because of the smaller volume of the chamber. Once the particle mass had reached a maximum in each experiment, three denuder-filter samples were taken. The solvent mixture for extraction of the denuder contents was replaced with methanol as dichloromethane was found to degrade the glue holding the annular spaces of the denuder together over time, causing the tubes to eventually break apart. A more efficient pre-concentration step was also employed which involved blowing down 1 mL of the filter extracts to near dryness using nitrogen and reconstituting them with 100 μ L of methanol. These solutions were then transferred to conical vial inserts and analyzed by GC-MS. Blank denuders and filters were prepared in the same way and extracted. Standard solutions were also used to quantify the photooxidation products in the gas and particle phases. Structurally similar compounds were used for those carbonyls which were not readily available.

2.3 GC-MS analysis

A Varian GC-MS system (Saturn 2000) equipped with a split/splitless injector (Varian 1079) was used for chemical analysis. The chromatographic column used was a Chrompack CP-Sil-8CB, (5% phenyl, 95% dimethylpolysiloxane), 30 m in length, with an internal diameter of 0.25 mm. The derivatives were analysed using the following column oven temperature program: 60°C held for 1 min, then ramped from 60°C to 100°C at 5°C min⁻¹, from 100°C to 280°C at 10°C min⁻¹ and from 280°C to 310°C at 30°C min⁻¹. The temperature was then held for 5 min. The injector temperature was held

4733

at 280°C for 1 min and then ramped to 310°C at 50°C min⁻¹. Mass spectra were acquired over a mass range m/z 60–650 amu in the electron ionization (EI) mode. When analysing the PFBHA derivatives, reconstructed ion chromatograms were used. The m/z =181 ion fragment was used in most cases for quantification of the derivatized carbonyls. However reconstructed ion chromatograms with more specific EI fragment ions were used whenever co-elution occurred.

2.4 Materials

The following compounds, with stated purities in brackets, were obtained from Sigma Aldrich Chemical Company; Amberlite XAD-4 resin, PFBHA (\geq 98%), methanol (99.9%), dichloromethane (\geq 99.8%), acetonitrile (99.9%), isoprene (99%), methacrolein (95%), methylvinylketone (99%), valeraldehyde (97%), glyoxal (40% in water), methylglyoxal (40% in water), 2,3-butanedione (97%), 3,5-dimethylbenzaldehyde (97%) and glyoxal trimer dihydrate (\geq 97%). The following compounds, with stated purities in brackets, were obtained from Fluka; 1,3,5-trimethylbenzene (99%), glycolaldehyde dimer (98%), hexane (\geq 98%). The following compounds, with stated purities in brackets, were obtained from Lancaster Synthesis (UK); hydroxyacetone (95%) and 2,5-hexanedione (97%). Nitric oxide (98.5%) was obtained from Sigma Aldrich Chemical Company.

3 Results and discussion

3.1 Concentration-time profiles and aerosol yields

The photooxidation of isoprene and 1,3,5-TMB was studied under a range of initial starting conditions, as indicated in Table 1. Typical concentration-time profiles obtained for experiments performed on isoprene and 1,3,5-TMB at PSI are shown in Figs. 2 and 3 respectively. The profiles for nitrogen oxides, ozone and particle mass were very

4734

similar in all experiments. As expected the decay of the hydrocarbon promotes the conversion of NO to NO₂ and the subsequent formation of ozone. SOA formation was observed after 80–140 min and coincided with the point at which all NO had been converted to NO₂. Following nucleation, the particles continued to grow due to condensation before reaching a maximum after about 300 min and then decreased due to wall losses. The particle mass was calculated from the measured volume concentration using a density of 1.4 g cm⁻³ which was determined by comparing the mobility diameter measurements from a differential mobility analyzer with the vacuum aerodynamic diameter measured with an online aerosol mass spectrometer (Dommen et al., 2006; Paulsen et al., 2005).

The formation of photooxidation products was monitored in real time using the PTR-MS, which detects VOCs in the form of the protonated molecular ion (M+1). In the isoprene experiments, the most abundant product ion appeared at $m/z=71$ and is attributed to the major first generation oxidation products, methacrolein (MACR) and methylvinylketone (MVK), which are isomers and cannot be distinguished in the PTR-MS. Additional major ions were also detected at the following m/z values and are tentatively attributed to the corresponding secondary products arising from further oxidation of MACR and MVK; 61 (glycolaldehyde), 75 (hydroxyacetone), 59 (glyoxal) and 73 (methylglyoxal). All of these carbonyls have previously been identified as primary or secondary products of isoprene photooxidation (Carter, 1996; Yu et al., 1995) and are consistent with the current understanding of the atmospheric degradation mechanism. In the 1,3,5-TMB experiments, the major product ion appeared at $m/z=113$ and could be due to any of the following species; *cis/trans* 2-methyl-4-oxo-2-pentenal, 3,5-dimethyl-5(2H)-2-furanone, 3,5-dimethyl-3(2H)-2-furanone, 3-methyl-furan-2, 5-dione. 2-methyl-4-oxo-2-pentenal has been previously observed as a photooxidation product of 1,3,5-TMB (Smith et al., 1999) but contributions from the other isomers are also possible. The other major ions were detected at $m/z=59$, 73, 135 and are attributed to the photooxidation products glyoxal, methylglyoxal, and 3,5-dimethylbenzaldehyde respectively. The PTR-MS instrument was calibrated using gas standards (Apel-Riemer

4735

Environmental Inc., Denver, CO) containing isoprene, methylvinylketone, methacrolein and 1,3,5-TMB and a total of 27 alcohols, ketones, and aldehydes. For compounds included in these standards an uncertainty of 5% is attributed to the data. For all oxygenated compounds in the gas standard an average sensitivity with an uncertainty of 30% was derived and applied to the other measured compounds.

Similar concentration-time profiles for nitrogen oxides, ozone and particle mass were also obtained in the experiments performed at UCC, Fig. 4. However, the rate of decay of the parent hydrocarbons and NO was almost doubled and the formation of particles, which was still coincident with the point at which all NO had been converted to NO₂, occurred earlier (after 30–45 min) than in the experiments performed at PSI. The increased rate of reaction in the UCC chamber is due to the higher light intensity around 360 nm which results in an increased photolysis rate for the OH radical precursor HONO generated from the reaction of NO_x at the walls of the reactor. It should also be noted that the wall loss rate of particles is higher in the UCC experiments due to the smaller volume to surface ratio in the chamber compared to PSI.

The yield of SOA produced in each experiment was calculated from the ratio of the aerosol mass formed to the amount of hydrocarbon reacted at the point where the maximum particle concentration was observed. The aerosol mass was corrected for wall losses by applying a first order loss rate obtained from the measured decay of the particles at the end of each experiment. The calculated yields are listed in Table 1 and, in general, show good agreement with previously reported SOA yields for these compounds (Cocker et al., 2001; Dommen et al., 2006). However, it is apparent that the yields obtained at PSI, particularly for the 1,3,5-TMB experiments, are slightly higher than those obtained in the UCC chamber. There are a number of factors that affect the yield of SOA in simulation chamber experiments including temperature, humidity, seed aerosol and concentration of NO_x. In both chambers, the experiments were performed in the absence of seed aerosol, at a relative humidity of around 50% and under high-NO_x conditions (>300 ppbV). For the experiments at PSI, the VOC to NO_x ratio was approximately 2:1, with roughly equal parts of NO and NO₂, whilst at UCC the

4736

VOC/NO_x ratio was around 4:1. The effect of NO_x on SOA yields is a complex issue and has been discussed in detail for the photooxidation of isoprene (Kroll et al., 2006) and aromatics (Ng et al., 2007). Although the total amount of NO_x was varied to some extent, no clear relationship was observed between the mixing ratio of NO_x and the SOA yield. This indicates that the variation in NO_x concentrations employed during the set of experiments reported in this work was not sufficient to cause a significant change in the SOA yields. The most likely explanation for the higher SOA yields in the PSI experiments is therefore the difference in temperature. The chamber at UCC does not have any cooling system and temperatures reached up to 32°C during photooxidation studies. At PSI experiments were carried out at 20°C and higher SOA yields may thus be expected due to more condensation of gas-phase products and thus addition of mass to the particle phase. It is interesting to note that this effect is more pronounced for 1,3,5-TMB, possibly indicating that the SOA contains more volatile species than those present in the SOA produced from isoprene photooxidation.

3.2 Denuder collection efficiency

The collection efficiency of the denuder was tested using the PTR-MS during the first isoprene (ISO_PSI_1) and 1,3,5-TMB (TMB_PSI_1) photooxidation experiments. Figure 5 shows how the PTR-MS signal changed when a PFBHA-coated denuder tube was placed in front of the inlet whilst sampling from the chamber. For the isoprene system, MACR and MVK (as well as isoprene) were efficiently trapped by the denuder tube as indicated by the dramatic decrease of the corresponding PTR-MS signals as air was sampled from the exit of the denuder tube. After a sampling time of 60 min there was still no breakthrough observed, indicating that these compounds were effectively collected by the denuder throughout this period. For the 1,3,5-TMB system, both glyoxal and methylglyoxal were efficiently trapped over a 150 min sampling period. Although the signal for 1,3,5-TMB initially dropped close to zero, it then gradually increased over this timeframe indicating that the denuder gradually became saturated with the parent VOC. It is important to note that even when breakthrough of 1,3,5-TMB was occurring,

4737

the signals for both glyoxal and methylglyoxal remained very close to zero indicating efficient collection of these carbonyls throughout the sampling period. Based on these results a sampling period of 50 min was chosen for the gas/particle partitioning studies in order to maximize the particle mass collected on the filter with minimal gas-phase breakthrough.

The collection efficiency of the denuder tube was also determined during each experiment at PSI using the F-D-D configuration, shown in Fig. 1. GC-MS data obtained for glyoxal and methylglyoxal in experiment ISO_PSI_1 are shown in Fig. 6. The results show that significant amounts of these dicarbonyls were collected on the filter and first denuder tube (Tube 1), while the amounts collected on Tube 2 were negligible. This confirms that gas-phase breakthrough of these compounds did not occur to any noticeable extent over a sampling period of 50 min and that the collection efficiency of the PFBHA-coated denuder tube was virtually 100% under the sampling conditions employed. In fact, for all of the carbonyls detected in the experiments at PSI and UCC, the amounts collected on the second tubes in both the F-D-D and D-F-D configurations were negligible.

3.3 Identification of photooxidation products by GC-MS

Denuder-filter sampling was employed 2–3 times during each experiment followed by GC-MS analysis of the denuder and filter extracts to identify carbonyl compounds present in the gas and particle phase respectively. Typical GC-MS data obtained from the photooxidation of isoprene and 1,3,5-TMB are shown in Figs. 7 and 8. The carbonyl compounds were identified by the retention times and mass spectra of their oxime derivatives (Yu et al., 1995, 1997) and are listed in Tables 2 and 3. All of these carbonyls have previously been observed (or tentatively identified) as gas-phase products in simulation chamber studies of the photooxidation of isoprene (Yu et al., 1995) and 1,3,5-TMB (Smith et al., 1999; Yu et al., 1997) using impingers containing aqueous solutions of PFBHA followed by GC-MS analysis of the oxime derivatives. However, no information on the composition of the particle phase was obtained in these studies.

4738

In the initial experiments performed at PSI, the full range of gas-phase products was identified in both the isoprene and 1,3,5-TMB systems, however, the only products found in the particle phase were glyoxal and methylglyoxal. In order to investigate the molecular composition of the particle phase further, experiments using higher mixing ratios of the parent hydrocarbon were performed at UCC. This approach, combined with the increased sensitivity provided by the pre-concentration step and the use of methanol as the extraction solvent, enabled the identification of several other products in the particle phase for both systems. In addition, the use of calibration solutions containing the oximes of the carbonyl products or appropriate surrogate compounds, allowed for estimation of the concentrations of the carbonyls formed. For the isoprene experiments MACR, MVK, glycolaldehyde, hydroxyacetone, glyoxal and methylglyoxal were quantified using their respective standards. The amount of 2-methyl-but-3-enal was determined using the response factor of the valeraldehyde derivative and oxopropanedial, hydroxypropanedial, methylbutenedial and butenedial were quantified using 2,3-butanedione as the surrogate compound. For the 1,3,5-TMB experiments 3,5-dimethylbenzaldehyde, glyoxal, and methylglyoxal were quantified using their respective standards. 2,3-dioxobutanal, oxopropanedial and butenedial were quantified using the response factor of the 2,3-butanedione derivative while 3-hydroxy-2,4-pentanedione, 2-methyl-4-oxo-2-pentenal and methylbutenedial were quantified using 2,5-hexanedione as the surrogate compound.

Mechanisms for the formation of the isoprene photooxidation products listed in Table 2 are well established. MACR and MVK are the major primary products formed from addition of OH to either of the double bonds in isoprene, followed by oxidation of the corresponding hydroxyalkyl radicals. The unsaturated C₅ carbonyl 2-methyl-but-3-enal can also be formed as a primary product in this way although with much lower yields than MACR and MVK (Fan and Zhang, 2004). Further reaction of MACR and MVK with OH leads to the formation of secondary products including glyoxal, methylglyoxal, glycolaldehyde and hydroxyacetone (Spaulding et al., 2003). Yu et al. proposed that 2-methylbutenedial and hydroxymethylglyoxal are formed through the reaction of OH

4739

with the primary isoprene photooxidation products 3-methylfuran and hydroxybut-3-en-2-one respectively (Yu et al., 1995). Oxopropanedial and butenedial are more difficult to explain mechanistically, and although these products (or their corresponding structural isomers) were tentatively identified by Yu et al. they were only observed during ozonolysis experiments (Yu et al., 1995). Interestingly, MACR, MVK and 2-methylbut-3-enal were only observed in the gas-phase, while all the other products were observed in both gas and particle phases. This indicates that SOA formation does not occur from direct condensation of the primary oxidation products, but instead, through further reaction of these species, in agreement with recent studies (Kroll et al., 2006; Ng et al., 2006).

Mechanisms for the formation of the 1,3,5-TMB photooxidation products listed in Table 3 are also fairly well established. 3,5-Dimethylbenzaldehyde is formed by H atom abstraction from one of the methyl groups in the parent hydrocarbon and has been observed as its PFBHA derivative in a previous study (Yu et al., 1997). Also observed in that study were the mechanistically expected primary ring-opened co-products methylglyoxal and 2-methyl-4-oxo-2-pentenal. It was proposed that 3-hydroxy-2,4-pentanedione is a secondary product resulting from further reaction of 2-methyl-4-oxo-2-pentenal and that the triones, oxopropanedial and 2,3-dioxobutanal are formed through the OH-initiated oxidation of hydroxydicarbonyls (Yu et al., 1997). The observation of 2-methylbutenedial and butenedial exclusively in the particle phase in this work is unexpected. However, their gas-phase concentrations could be below the limits of detection for the method considering a pre-concentration step was not employed for the denuder extracts. Although 2-methylbutenedial was observed as a photooxidation product of 1,3,5-TMB by Yu et al., its formation cannot be easily explained. 2-methylbutenedial and butenedial are major primary products from the photooxidation of benzene, toluene, m- and p-xylene and 1,2,4-TMB (Yu et al., 1997) and could therefore arise from low level impurities in the 1,3,5-TMB sample used in this work. Small amounts of glyoxal were detected in the gas phase, but since this dicarbonyl cannot be formed as a primary ring-opened product due to the position of the methyl groups on

4740

1,3,5-TMB, it seems likely that it is formed via secondary reactions, or from oxidation of impurities in the 1,3,5-TMB sample, as for 2-methylbutenedial and butenedial.

The quantification procedure was used to determine yields for the carbonyl compounds detected in the particle phase. The corresponding gas-phase yields were not estimated since denuder-filter sampling was performed only during the latter stages of the photooxidation process when secondary chemistry was dominant. The particle-phase yields shown in Tables 2 and 3 are based on the average of 3 samples. For the isoprene system the identified carbonyls can only account for around 5% of the SOA mass. A significant amount of the SOA mass (22–34%) produced from the photooxidation of isoprene under high-NO_x conditions has been attributed to oligomers arising from oxidation of MACR (Surratt et al., 2006). A range of other polar organics including tetrols and acids are also present in isoprene SOA (Claeys et al., 2004; Surratt et al., 2006), but the yields of these species are difficult to determine. For the 1,3,5-TMB system the identified carbonyls can account for almost 10% of the SOA mass. This compares favourably with the work of Hamilton et al. who attributed around 10% of the mass of toluene SOA to small oxygenated compounds (Hamilton et al., 2005). A dominant fraction of the 1,3,5-TMB SOA mass is also believed to be due to oligomers arising from heterogeneous reaction of oxidation products (Kalberer et al., 2004).

3.3.1 Gas/particle partitioning of photooxidation products

Experimental gas/particle partitioning coefficients, $K_{p,i}$ (experimental), were calculated using the following expression (Odum et al., 1996):

$$K_{p,i}(\text{experimental}) = \frac{C_{p,i}}{C_{g,i}TSP} \quad (1)$$

where $C_{g,i}$ and $C_{p,i}$ are the relative concentrations of each product in the denuder (gas phase) and filter (particle phase) extracts, and TSP is the total suspended particulate concentration or average particle mass concentration ($\mu\text{g m}^{-3}$) measured during the

4741

sampling period. For comparison purposes theoretical $K_{p,i}$ values were also calculated using standard absorptive gas/particle partitioning theory (Pankow, 1994a, 1994b):

$$K_{p,i}(\text{theoretical}) = \frac{760 RT f_{om}}{MW_{om} 10^6 \zeta_i p_{L,i}^\circ} \quad (2)$$

where f_{om} is the mass fraction of the TSP that is the absorbing organic material (om) phase, MW_{om} is the average molecular weight of the absorbing om (g mol^{-1}), ζ_i is the activity coefficient of compound i in the om phase and $p_{L,i}^\circ$ is the vapour pressure (Torr) of the absorbing compound as a liquid, R is the ideal gas constant ($8.206 \times 10^{-5} \text{ m}^3 \text{ atm mol}^{-1} \text{ K}^{-1}$) and T is the temperature (K) taken to be 293 K and 305 K in the experiments performed at PSI and UCC respectively. Liquid vapour pressure values were estimated using the SPARC online calculator (Version 3.1) (Hilal et al., 1995), a group contribution calculation procedure that has been used to estimate vapour pressure values for a range of organic compounds in previous studies (Asher et al., 2002; Barsanti and Pankow, 2004, 2005, 2006). The values of f_{om} and ζ_i were assumed to be 1, as in previous studies (Johnson et al., 2006; Kamens et al., 1999), and MW_{om} is estimated arbitrarily to be 120 for all experiments in this study (Jang and Kamens, 2001). The units of $K_{p,i}$ are $\text{m}^3 \mu\text{g}^{-1}$ and experimental and theoretical $K_{p,i}$ values for the isoprene and 1,3,5-TMB photooxidation products are compared in Tables 4 and 5 respectively.

The experimental $K_{p,i}$ values obtained for glyoxal and methylglyoxal in the two simulation chambers for the isoprene and 1,3,5-TMB systems are in reasonable agreement. The reproducibility of experimental $K_{p,i}$ values is improved for the experiments at UCC due to the pre-concentration of filter extracts and the higher precursor concentrations used. This is the first reported study of gas/particle partitioning in the photooxidation of isoprene and 1,3,5-TMB and a direct comparison with literature values is therefore not possible. However, the values obtained here are broadly in line with the experimental $K_{p,i}$ values determined for a number of different carbonyls in the atmospheric oxidation of toluene (Jang and Kamens, 2001), α -pinene (Kamens and Jaoui, 2001) and other biogenic precursors (Yu et al., 1999).

4742

The main feature of the results presented in Tables 4 and 5 is that the experimental $K_{p,i}$ values are much higher than their theoretical counterparts, particularly for the dicarbonyl species glyoxal and methylglyoxal. This provides further evidence to support the view that transfer to the particle phase is not occurring by gas/particle partitioning alone and that the heterogeneous reactions of dicarbonyls are important in SOA formation and growth (Kalberer et al., 2004; Liggio et al., 2005b). The reactive uptake of glyoxal into particles has been observed in several previous studies and has been explained by hydration reactions occurring on/in the particle phase leading to larger low-volatility products (Hastings et al., 2005; Jang et al., 2002; Liggio et al., 2005a). Similar hydration reactions have been observed when evaporating aqueous solutions of glyoxal and methylglyoxal (Loeffler et al., 2006). The formation of oligomers has also been recently observed in the photooxidation of both isoprene (Dommen et al., 2006; Surratt et al., 2006) and 1,3,5-TMB (Kalberer et al., 2004). In the latter case, oligomers attributed to the heterogeneous reactions of methylglyoxal and other carbonyl products, were found to comprise over 50% of the SOA mass after ageing for 20 h (Kalberer et al., 2004). Oligomer formation has recently been observed from the atmospheric oxidation of a variety of precursors (Dommen et al., 2006; Hamilton et al., 2006; Kalberer et al., 2004; Tolocka et al., 2004; Zahardis et al., 2006) and it has become clear that heterogeneous processes are an important pathway for SOA growth.

The experiments performed in this work are very similar to those previously performed at the PSI chamber where oligomer formation was observed, and as a result the filter samples collected in these experiments are also expected to contain oligomeric material. However, oligomers have not been detected by GC-MS before, possibly due to the high temperatures typically used in the analytical procedure. Furthermore, there is evidence to support the fact that the oligomers can revert to their monomeric form in solution. Indeed, tests performed at UCC showed that methanol containing PFBHA was found to efficiently dissolve a trimeric glyoxal standard and convert the resulting monomers to oxime derivatives. If glyoxal – or methylglyoxal-based oligomers were present in the particle phase, then reversion to the monomeric form in the extracts

4743

would be expected. Indeed, if the oligomerization process is assumed to be reversible, the use of excess PFBHA would be expected to convert the oligomers back to the monomeric species by removing dicarbonyl monomers from the extract as soon as they are formed.

The results presented in Tables 4 and 5 indicate that the deviation from absorptive gas/particle partitioning theory is greatest for glyoxal, methylglyoxal and dialdehydes in general. In fact, with the exception of 3-hydroxy-2,4-pentanedione, all of the dicarbonyls were observed to transfer to the particle phase more effectively than products with a single carbonyl moiety. For example MACR and MVK, although present at relatively high mixing ratios in the gas phase during the isoprene experiments, were not observed in any of the filter extracts. Indeed, Barsanti and Pankow predicted accretion reactions involving straight-chain aldehydes up to C_{10} to be thermodynamically unfavourable under atmospheric conditions (Barsanti and Pankow, 2004). Barsanti and Pankow followed this study with a second focusing on the thermodynamic potential of dicarbonyls to add mass to ambient particulate matter through accretion reactions, using an initial background organic particulate matter concentration of $15 \mu\text{gm}^{-3}$ for their calculations (Barsanti and Pankow, 2005). Glyoxal and methylglyoxal in particular were expected to have an effect on particulate matter mass loading through hydration/oligomerization and aldol condensation reactions respectively. Interestingly, in that study the contribution of these two dicarbonyls to the particle phase was predicted to be almost equal, and the experimental $K_{p,i}$ values calculated in this work are also on a similar order of magnitude with respect to each other. However, glyoxal does exhibit consistently higher experimental $K_{p,i}$ values than methylglyoxal indicating that the dominating accretion reactions for the dialdehyde may be occurring at a higher rate. Experimental $K_{p,i}$ values for hydroxycarbonyl photooxidation products agreed more closely with their theoretical values based on absorptive partitioning, in particular for 3-hydroxy-2,4-pentanedione, which does not possess an aldehyde functionality and is thus expected to be less reactive. This is in agreement with Barsanti and Pankow who predicted that diketones such as 2,3-butanedione and 2,5-hexanedione would con-

4744

tribute much less to the growth of SOA via accretion reactions because of the lower reactivity of ketones compared to their aldehyde counterparts (Barsanti and Pankow, 2005).

The importance of determining experimental partitioning values is underlined by recent modelling studies of SOA formation from anthropogenic and biogenic precursors in simulation chamber experiments where all gas/particle partitioning coefficients of oxidation products had to be scaled by a species-independent factor of between 5 and 120 to explain the SOA mass formed (Jenkin, 2004; Johnson et al., 2005). A simulation of regional scale SOA formation in the UK required gas/particle partitioning coefficients of oxidation products to be scaled by a factor of 500 (Johnson et al., 2006). The results of this work suggest that different scaling factors, based on the experimental $K_{p,i}$ values, should be used for each compound, or at least each group of compounds.

4 Conclusions

Experimental gas/particle partitioning coefficients for a wide range of carbonyl products formed from the photooxidation of isoprene and 1,3,5-TMB were found to deviate to varying extents from their theoretical values based on standard absorptive partitioning theory. Photooxidation products with a single carbonyl moiety were not observed in the particle phase, but dicarbonyls, and in particular, glyoxal and methylglyoxal, exhibited gas/particle partitioning coefficients several orders of magnitude higher than expected theoretically. These findings support the importance of heterogeneous chemistry as a pathway for SOA formation and growth during the atmospheric degradation of anthropogenic and biogenic precursors.

Acknowledgements. This work was supported by the European Commission (project EU-ROCHAMP, contract number RII3-CT-2004-505968) and the ACCENT "Access to Infrastructures" programme. The authors would like to thank J. M. S. Lopez for his assistance in operating the GC-MS instrument at UCC.

4745

References

- Asher, W. E., Pankow, J. F., Erdakos, G. B., and Seinfeld, J. H.: Estimating the vapor pressures of multi-functional oxygen-containing organic compounds using group contribution methods, *Atmos. Environ.*, 36(9), 1483–1498, 2002.
- Barsanti, K. C. and Pankow, J. F.: Thermodynamics of the formation of atmospheric organic particulate matter by accretion reactions - Part 1: aldehydes and ketones, *Atmos. Environ.*, 38(26), 4371–4382, 2004.
- Barsanti, K. C. and Pankow, J. F.: Thermodynamics of the formation of atmospheric organic particulate matter by accretion reactions – Part 2: Dialdehydes, methylglyoxal, and diketones, *Atmos. Environ.*, 39(35), 6597–6607, 2005.
- Barsanti, K. C. and Pankow, J. F.: Thermodynamics of the formation of atmospheric organic particulate matter by accretion reactions – Part 3: Carboxylic and dicarboxylic acids, *Atmos. Environ.*, 40(34), 6676–6686, 2006.
- Carter, W. P. L.: Condensed atmospheric photooxidation mechanisms for isoprene, *Atmos. Environ.*, 30(24), 4275–4290, 1996.
- Claeys, M., Graham, B., Vas, G., et al.: Formation of secondary organic aerosols through photooxidation of isoprene, *Science*, 303(5661), 1173–1176, 2004.
- Cocker, D. R., Mader, B. T., Kalberer, M., Flagan, R. C., and Seinfeld, J. H.: The effect of water on gas/particle partitioning of secondary organic aerosol: II. m-xylene and 1,3,5-trimethylbenzene photooxidation systems, *Atmos. Environ.*, 35(35), 6073–6085, 2001.
- Dommen, J., Metzger, A., Duplissy, J., et al.: Laboratory observation of oligomers in the aerosol from isoprene/NO_x photooxidation, *Geophys. Res. Lett.*, 33(13), L13805, doi:10.1029/2006, 2006.
- Edney, E. O., Kleindienst, T. E., Jaoui, M., et al.: Formation of 2-methyl tetrols and 2-methylglyceric acid in secondary organic aerosol from laboratory irradiated isoprene/NO_x/SO₂/air mixtures and their detection in ambient PM_{2.5} samples collected in the eastern United States, *Atmos. Environ.*, 39(29), 5281–5289, 2005.
- Fan, J. and Zhang, R.: Atmospheric Oxidation Mechanism of Isoprene, *Environ. Chem.*, 1, 140–149, 2004.
- Forstner, H. J. L., Flagan, R. C., and Seinfeld, J. H.: Secondary organic aerosol from the photooxidation of aromatic hydrocarbons: Molecular composition, *Environ. Sci. Technol.*, 31(5), 1345–1358, 1997.

4746

- Fuzzi, S., Andreae, M. O., Huebert, B. J., et al.: Critical assessment of the current state of scientific knowledge, terminology, and research needs concerning the role of organic aerosols in the atmosphere, climate, and global change, *Atmos. Chem. Phys.*, 6, 2017–2038, 2006, <http://www.atmos-chem-phys.net/6/2017/2006/>.
- 5 Hamilton, J. F., Lewis, A. C., Reynolds, J. C., Carpenter, L. J., and Lubben, A.: Investigating the composition of organic aerosol resulting from cyclohexene ozonolysis: low molecular weight and heterogeneous reaction products, *Atmos. Chem. Phys.*, 6, 4973–4984, 2006, <http://www.atmos-chem-phys.net/6/4973/2006/>.
- 10 Hamilton, J. F., Webb, P. J., Lewis, A. C., and Reviejo, M. M.: Quantifying small molecules in secondary organic aerosol formed during the photo-oxidation of toluene with hydroxyl radicals, *Atmos. Environ.*, 39(38), 7263–7275, 2005.
- Hastings, W. P., Koehler, C. A., Bailey, E. L., and DeHaan, D. O.: Secondary Organic Aerosol Formation by Glyoxal Hydration and Oligomer Formation: Humidity Effects and Equilibrium Shifts during Analysis, *Environ. Sci. Technol.*, 39(22), 8728–8735, 2005.
- 15 Hilal, S. H., Karickhoff, S. W., and Carreira, L. A.: A rigorous test for SPARC's chemical reactivity models: Estimation of more than 4300 ionization pK(a)s, *Quantitative Structure-Activity Relationships*, 14(4), 348–355, 1995.
- Jang, M. S., Czoschke, N. M., Lee, S., and Kamens, R. M.: Heterogeneous atmospheric aerosol production by acid-catalyzed particle-phase reactions, *Science*, 298(5594), 814–817, 2002.
- 20 Jang, M. S. and Kamens, R. M.: Characterization of secondary aerosol from the photooxidation of toluene in the presence of NO_x and 1-propene, *Environ. Sci. Technol.*, 35(18), 3626–3639, 2001.
- Jenkin, M. E.: Modelling the formation and composition of secondary organic aerosol from alpha- and beta-pinene ozonolysis using MCM v3, *Atmos. Chem. Phys.*, 4, 1741–1757, 2004.
- 25 Johnson, D., Jenkin, M. E., Wirtz, K., and Martin-Reviejo, M.: Simulating the formation of secondary organic aerosol from the photooxidation of aromatic hydrocarbons, *Environ. Chem.*, 2(1), 35–48, 2005.
- 30 Johnson, D., Utembe, S. R., Jenkin, M. E., et al.: Simulating regional scale secondary organic aerosol formation during the TORCH 2003 campaign in the southern UK, *Atmos. Chem. Phys.*, 6, 403–418, 2006, <http://www.atmos-chem-phys.net/6/403/2006/>.

4747

- Kalberer, M., Paulsen, D., Sax, M., et al.: Identification of polymers as major components of atmospheric organic aerosols, *Science*, 303(5664), 1659–1662, 2004.
- Kamens, R., Jang, M., Chien, C. J., and Leach, K.: Aerosol formation from the reaction of alpha-pinene and ozone using a gas-phase kinetics aerosol partitioning model, *Environ. Sci. Technol.*, 33(9), 1430–1438, 1999.
- 5 Kamens, R. M. and Jaoui, M.: Modeling aerosol formation from alpha-pinene plus NO_x in the presence of natural sunlight using gas-phase kinetics and gas-particle partitioning theory, *Environ. Sci. Technol.*, 35(7), 1394–1405, 2001.
- Kanakidou, M., Seinfeld, J. H., Pandis, S. N., et al.: Organic aerosol and global climate modelling: a review, *Atmos. Chem. Phys.*, 5, 1053–1123, 2005, <http://www.atmos-chem-phys.net/5/1053/2005/>.
- 10 Kleindienst, T. E., Edney, E. O., Lewandowski, M., Offenberger, J. H., and Jaoui, M.: Secondary organic carbon and aerosol yields from the irradiations of isoprene and alpha-pinene in the presence of NO_x and SO₂, *Environ. Sci. Technol.*, 40(12), 3807–3812, 2006.
- 15 Kroll, J. H., Ng, N. L., Murphy, S. M., Flagan, R. C., and Seinfeld, J. H.: Secondary organic aerosol formation from isoprene photooxidation, *Environ. Sci. Technol.*, 40(6), 1869–1877, 2006.
- Liggio, J., Li, S. M., and McLaren, R.: Heterogeneous reactions of glyoxal on particulate matter: Identification of acetals and sulfate esters, *Environ. Sci. Technol.*, 39(6), 1532–1541, 2005a.
- 20 Liggio, J., Li, S. M., and McLaren, R.: Reactive uptake of glyoxal by particulate matter, *J. Geophys. Res.-Atmos.*, 110(D10), D10304, doi:10.1029/2004/JD005113, 2005b.
- Loeffler, K. W., Koehler, C. A., Paul, N. M., and DeHaan, D. O.: Oligomer Formation in Evaporating Aqueous Glyoxal and Methyl Glyoxal Solutions, *Environ. Sci. Technol.*, 40(20), 6318–6323, 2006.
- 25 Ng, N. L., Kroll, J. H., Chan, A. W. H., et al.: Secondary organic aerosol formation from m-xylene, toluene, and benzene, *Atmos. Chem. Phys.*, 7(14), 3909–3922, 2007.
- Ng, N. L., Kroll, J. H., Keywood, M. D., et al.: Contribution of first- versus second-generation products to secondary organic aerosols formed in the oxidation of biogenic hydrocarbons, *Environ. Sci. Technol.*, 40(7), 2283–2297, 2006.
- 30 Odum, J. R., Hoffmann, T., Bowman, F., et al.: Gas/particle partitioning and secondary organic aerosol yields, *Environ. Sci. Technol.*, 30(8), 2580–2585, 1996.
- Odum, J. R., Jungkamp, T. P. W., Griffin, R. J., Flagan, R. C., and Seinfeld, J. H.: The atmospheric aerosol-forming potential of whole gasoline vapor, *Science*, 276(5309), 96–99,

4748

- 1997.
- Pankow, J. F.: An Absorption-Model of Gas-Particle Partitioning of Organic-Compounds in the Atmosphere, *Atmos. Environ.*, 28(2), 185–188, 1994a.
- Pankow, J. F.: An Absorption-Model of the Gas Aerosol Partitioning Involved in the Formation of Secondary Organic Aerosol, *Atmos. Environ.*, 28(2), 189–193, 1994b.
- Paulsen, D., Dommen, J., Kalberer, M., et al.: Secondary organic aerosol formation by irradiation of 1,3,5-trimethylbenzene-NO_x-H₂O in a new reaction chamber for atmospheric chemistry and physics, *Environ. Sci. Technol.*, 39(8), 2668–2678, 2005.
- Pöschl, U.: Atmospheric aerosols: Composition, transformation, climate and health effects, *Angewandte Chemie-International Edition*, 44(46), 7520–7540, 2005.
- Smith, D. F., Kleindienst, T. E., and McIver, C. D.: Primary product distributions from the reaction of OH with m-, p-xylene, 1,2,4- and 1,3,5-trimethylbenzene, *J. Atmos. Chem.*, 34(3), 339–364, 1999.
- Spaulding, R. S., Schade, G. W., Goldstein, A. H., and Charles, M. J.: Characterization of secondary atmospheric photooxidation products: Evidence for biogenic and anthropogenic sources, *J. Geophys. Res.-Atmos.*, 108(D8), 4247, doi:10.1029/2002JD002478, 2003.
- Surratt, J. D., Murphy, S. M., Kroll, J. H., et al.: Chemical composition of secondary organic aerosol formed from the photooxidation of isoprene, *J. Phys. Chem. A*, 110(31), 9665–9690, 2006.
- Temime, B., Healy, R. M., and Wenger, J. C.: A Denuder-Filter Sampling Technique for the Detection of Gas and Particle Phase Carbonyl Compounds, *Environ. Sci. Technol.*, 41(18), 6514–6520, 2007.
- Tolocka, M. P., Jang, M., Ginter, J. M., et al.: Formation of oligomers in secondary organic aerosol, *Environ. Sci. Technol.*, 38(5), 1428–1434, 2004.
- Yu, J. Z., Cocker, D. R., Griffin, R. J., Flagan, R. C., and Seinfeld, J. H.: Gas-phase ozone oxidation of monoterpenes: Gaseous and particulate products. *J. Atmos. Chem.*, 34(2), 207–258, 1999.
- Yu, J. Z., Jeffries, H. E., and Lelacheur, R. M.: Identifying Airborne Carbonyl-Compounds in Isoprene Atmospheric Photooxidation Products by Their PFBHA Oximes Using Gas-Chromatography Ion-Trap Mass-Spectrometry, *Environ. Sci. Technol.*, 29(8), 1923–1932, 1995.
- Yu, J. Z., Jeffries, H. E., and Sexton, K. G.: Atmospheric photooxidation of alkylbenzenes, 1. Carbonyl product analyses, *Atmos. Environ.*, 31(15), 2261–2280, 1997.

4749

Zahardis, J., LaFranchi, B. W., and Petrucci, G. A.: Direct observation of polymerization in the oleic acid-ozone heterogeneous reaction system by photoelectron resonance capture ionization aerosol mass spectrometry, *Atmos. Environ.*, 40(9), 1661–1670, 2006.

Table 1. Starting concentrations and results for the isoprene and 1,3,5-TMB photooxidation experiments.

Experiment	[HC] ₀ (ppbV)	[NO] ₀ (ppbV)	[NO ₂] ₀ (ppbV)	Δ[HC] ^a (ug m ⁻³)	Aerosol Mass ^b (ug m ⁻³)	Aerosol Yield ^c (%)
ISO_PSI_1	1776	446	488	4283	203	4.72
ISO_PSI_2	1473	344	365	3959	189	4.76
ISO_UCC_1	2011	390	106	5140	220	4.29
ISO_UCC_2	4079	686	269	10541	467	4.43
TMB_PSI_1	815	194	177	1822	110	6.01
TMB_PSI_2	1027	335	289	2488	208	8.34
TMB_PSI_3	1017	286	294	2673	195	7.28
TMB_UCC_1	1193	246	21	3137	141	4.50
TMB_UCC_2	2929	496	100	7039	359	5.10

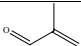
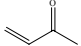
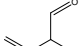
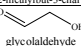
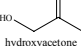
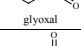
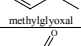
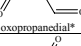
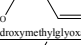
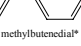
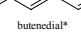
^a Amount of parent hydrocarbon (HC) reacted, corrected for dilution due to sampling.

^b Determined at the time of measured maximum particle volume concentration, corrected for wall loss, assuming a density of 1.4 g cm⁻³.

^c Calculated from aerosol mass/Δ[HC].

4751

Table 2. Gas- and particle-phase products observed by GC-MS during the photooxidation of isoprene.

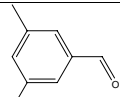
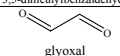
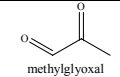
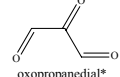
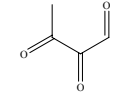
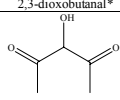
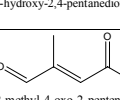
Compound	Retention time (min)	Molecular mass of derivative	m/z (EI mode)	Gas phase	Particle Phase (% Yield) ^a
 methacrolein	12.69	265	181 265 (M)	Yes	No
 methyl vinyl ketone	12.82, 12.87	265	181 265(M)	Yes	No
 2-methylbut-3-enal*	13.24, 13.32	279	181 279 (M)	Yes	No
 glycolaldehyde	14.14, 14.53	255	181 255 (M) 238 (M-17)	Yes	1.00 ± 0.26
 hydroxyacetone	14.73	269	181 269 (M) 252 (M-17)	Yes	1.29 ± 0.54
 glyoxal	21.13, 21.22	448	181 448 (M) 251 (M-197)	Yes	1.11 ± 0.24
 methylglyoxal	21.24, 21.51	462	181 462 (M) 265 (M-197)	Yes	1.04 ± 0.34
 oxopropanedial*	21.65, 21.71, 22.19, 22.23	476	181 476 (M) 279 (M-197)	Yes	0.10 ± 0.05
 hydroxymethylglyoxal*	22.90, 23.02	478	181 478 (M) 281 (M-197)	Yes	0.10 ± 0.04
 methylbutenedial*	25.80, 25.86, 26.25, 26.73, 26.94	488	181 488 (M) 307 (M-181)	Yes	0.27 ± 0.07
 butenedial*	27.16	474	181 474 (M)	Yes	0.25 ± 0.10

* No standard available. Product tentatively identified on the basis of retention time and mass spectrum.

^a Contribution of each carbonyl to the average SOA mass taken from the average of three individual samples taken during experiment ISO.UCC.2. Quoted errors correspond to the relative standard deviation of the three samples.

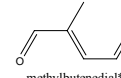
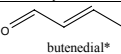
4752

Table 3. Gas- and particle-phase products observed by GC-MS during the photooxidation of 1,3,5-TMB.

Compound	Retention time (min)	Molecular weight of derivative	<i>m/z</i> (EI mode)	Gas phase	Particle Phase (% Yield) ^a
 3,5-dimethylbenzaldehyde	20.40, 20.48	329	181 329 (M) 299 (M-30)	Yes	No
 glyoxal	21.13, 21.22	448	181 448 (M) 251 (M-197)	Yes	No
 methylglyoxal	20.66, 21.14, 21.26, 21.40	462	181 462 (M) 265 (M-197)	Yes	2.06 ± 0.08
 oxopropanedial*	21.65	476	181 476 (M) 279 (M-197)	Yes	0.92 ± 0.07
 2,3-dioxobutanal*	21.85, 22.10	490	181 490 (M) 293 (M-197)	Yes	0.55 ± 0.14
 3-hydroxy-2,4-pentanedione*	22.98, 23.20	506	181 506 (M) 489 (M-17) 309 (M-197)	Yes	1.27 ± 0.02
 2-methyl-4-oxo-2-pentenal*	23.41, 23.75, 24.53, 25.38, 25.51, 25.61, 26.16	502	181 502 (M) 321 (M-181)	Yes	2.59 ± 0.12

4753

Table 3. Continued.

 methylbutenedial*	26.25, 26.73	488	181 488 (M) 307 (M-181)	No	0.59 ± 0.07
 butenedial*	27.16	474	181 474 (M)	No	1.67 ± 0.19

* No standard available. Product tentatively identified on the basis of retention time and mass spectrum.

^a Contribution of each carbonyl to the average SOA mass taken from the average of three individual samples taken during experiment TMB_UCC.2. Quoted errors correspond to the relative standard deviation of the three samples.

4754

Table 4. Experimental and theoretical gas/particle partitioning coefficients for isoprene photooxidation products.

Experiment	Compound	n	$K_{p,i}$ (experimental) ^a	$K_{p,i}$ (theoretical)	$K_{p,i}(\text{experimental}) /$ $K_{p,i}(\text{theoretical})$
ISO_PSI_2	glyoxal	2	$(7.34 \pm 0.60) \times 10^{-5}$	1.93×10^{-9}	38031
	methylglyoxal	2	$(9.96 \pm 1.78) \times 10^{-6}$	4.14×10^{-9}	2405
ISO_UCC_1	glyoxal	3	$(6.25 \pm 1.33) \times 10^{-5}$	9.75×10^{-10}	64102
	methylglyoxal	3	$(1.14 \pm 0.10) \times 10^{-5}$	1.95×10^{-9}	5846
	methylbutenedial	3	$(3.62 \pm 4.77) \times 10^{-4}$	3.37×10^{-7}	1074
	butenedial	3	$(6.17 \pm 3.78) \times 10^{-4}$	1.55×10^{-7}	3980
ISO_UCC_2	glyoxal	3	$(4.44 \pm 1.46) \times 10^{-5}$	9.75×10^{-10}	45538
	methylglyoxal	3	$(6.78 \pm 2.68) \times 10^{-6}$	1.95×10^{-9}	3476
	methylbutenedial	3	$(7.85 \pm 1.76) \times 10^{-5}$	3.37×10^{-7}	232
	butenedial	3	$(4.06 \pm 2.08) \times 10^{-4}$	1.55×10^{-7}	2619
	glycolaldehyde	3	$(2.15 \pm 0.57) \times 10^{-5}$	3.60×10^{-7}	59
	hydroxyacetone	3	$(1.48 \pm 0.56) \times 10^{-5}$	7.20×10^{-7}	20
	oxopropanedial	3	$(7.51 \pm 3.52) \times 10^{-6}$	5.58×10^{-8}	134
	hydroxymethylglyoxal	3	$(2.19 \pm 0.45) \times 10^{-4}$	2.49×10^{-6}	88

^a Average value based on *n* measurements during each experiment. Quoted errors correspond to the relative standard deviation.

4755

Table 5. Experimental and theoretical gas/particle partitioning coefficients for 1,3,5-TMB photooxidation products.

Experiment	Compound	n	$K_{p,i}$ (experimental) ^a	$K_{p,i}$ (theoretical)	$K_{p,i}(\text{experimental}) /$ $K_{p,i}(\text{theoretical})$
TMB_PSI_1	methylglyoxal	1	5.89×10^{-5}	4.14×10^{-9}	14227
TMB_PSI_2	methylglyoxal	3	$(3.94 \pm 3.53) \times 10^{-5}$	4.14×10^{-9}	9517
TMB_PSI_3	methylglyoxal	2	$(2.0 \pm 0.07) \times 10^{-5}$	4.14×10^{-9}	4831
TMB_UCC_1	methylglyoxal	3	$(1.6 \pm 0.90) \times 10^{-5}$	1.95×10^{-9}	8667
	oxopropanedial	3	$(1.90 \pm 1.70) \times 10^{-5}$	5.58×10^{-8}	341
	3-hydroxy-2,4-pentanedione	3	$(1.09 \pm 0.36) \times 10^{-4}$	1.13×10^{-5}	9
	2-methyl-4-oxo-2-pentenal	3	$(1.01 \pm 0.72) \times 10^{-4}$	9.32×10^{-7}	108
TMB_UCC_2	methylglyoxal	3	$(1.22 \pm 0.05) \times 10^{-5}$	1.95×10^{-9}	6256
	oxopropanedial	3	$(4.15 \pm 0.23) \times 10^{-5}$	5.58×10^{-8}	744
	2,3-dioxobutanal	3	$(1.20 \pm 0.56) \times 10^{-5}$	8.48×10^{-8}	142
	3-hydroxy-2,4-pentanedione	3	$(1.40 \pm 0.49) \times 10^{-5}$	1.13×10^{-5}	1
	2-methyl-4-oxo-2-pentenal	3	$(1.77 \pm 0.50) \times 10^{-4}$	9.32×10^{-7}	190

^a Average value based on *n* measurements during each experiment. Quoted errors correspond to the relative standard deviation

4756

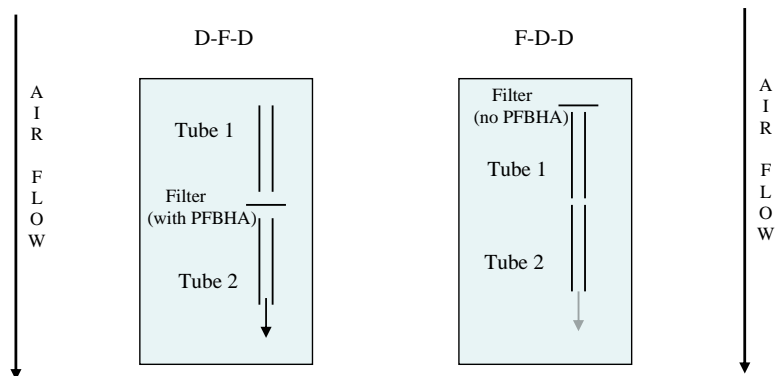


Fig. 1. The denuder-filter-denuder (D-F-D) and filter-denuder-denuder (F-D-D) sampling configurations used for determining gas/particle partitioning and gas-phase breakthrough respectively.

4757

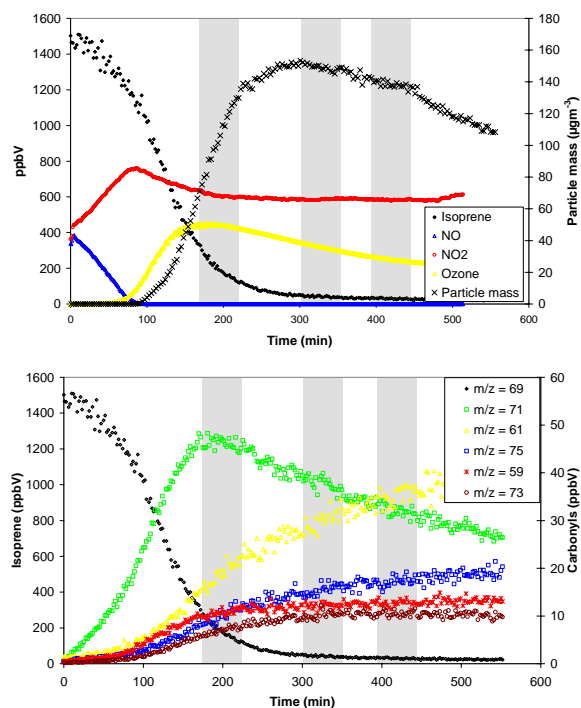


Fig. 2. Top: Concentration-time profile of isoprene, nitrogen oxides, ozone and particle mass for experiment ISO_PSI.2. Bottom: PTR-MS concentration-time data for isoprene and its oxidation products during experiment ISO_PSI.2. The grey areas represent the denuder-filter sampling periods.

4758

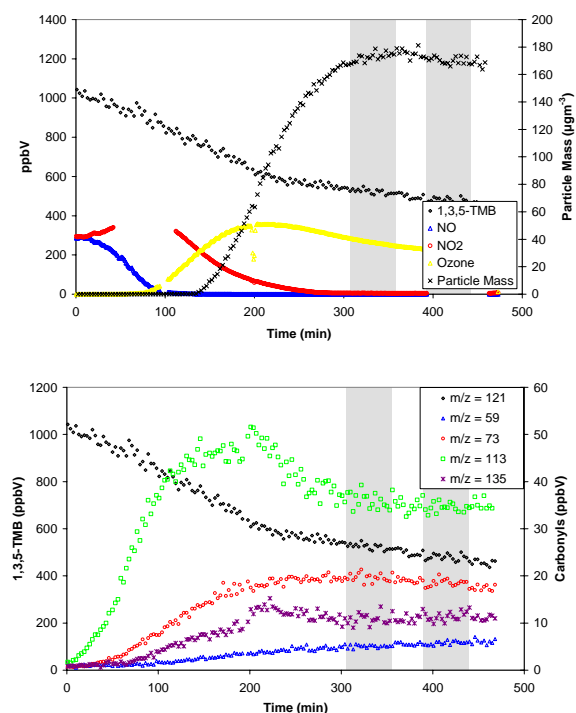


Fig. 3. Top: Concentration-time profile of 1,3,5-TMB, nitrogen oxides, ozone and particle mass for experiment TMB_PSI.3. Bottom: PTR-MS concentration-time data for 1,3,5-TMB and its oxidation products during experiment TMB_PSI.3. The grey areas represent the denuder-filter sampling periods.

4759

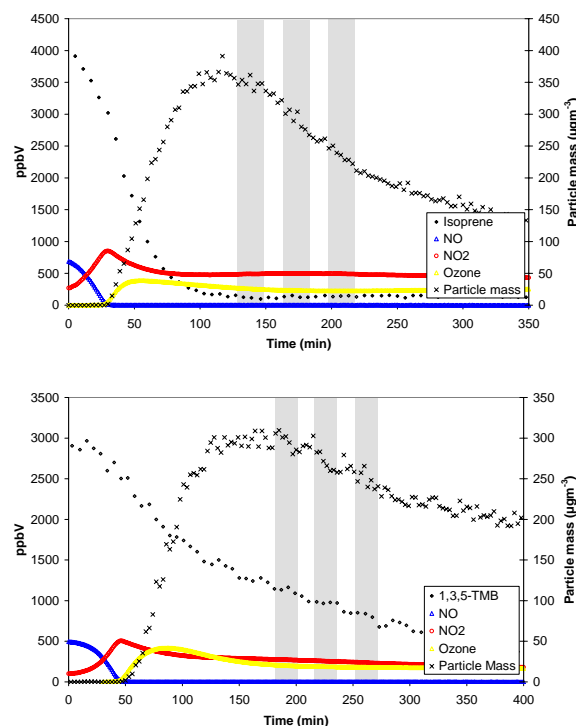


Fig. 4. Concentration-time profile of parent hydrocarbon, nitrogen oxides, ozone and particle mass for experiments ISO.UCC.2 (top) and TMB.UCC.2 (bottom). The grey areas represent the denuder-filter sampling periods.

4760

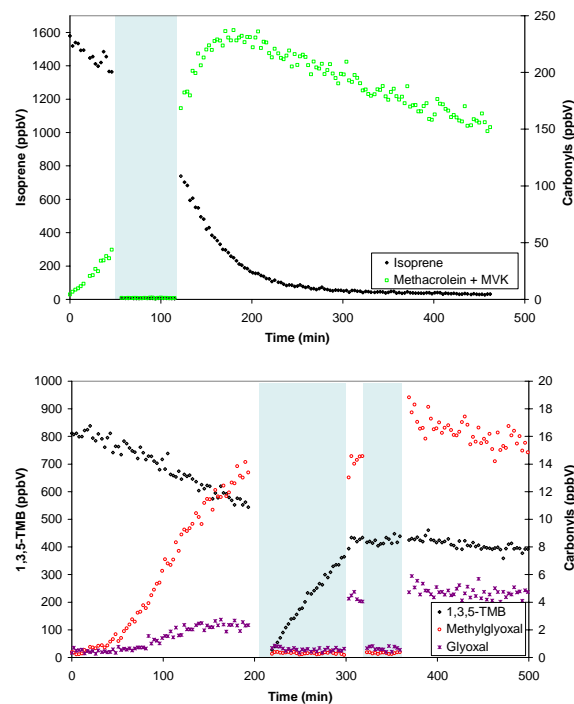


Fig. 5. PTR-MS Concentration-time profiles for isoprene, methacrolein and methylvinylketone (ISO_PSI_1), and 1,3,5-TMB, glyoxal and methylglyoxal (TMB_PSI_1). The shaded areas depict the periods when the PTR-MS sampled from the denuder tube exit.

4761

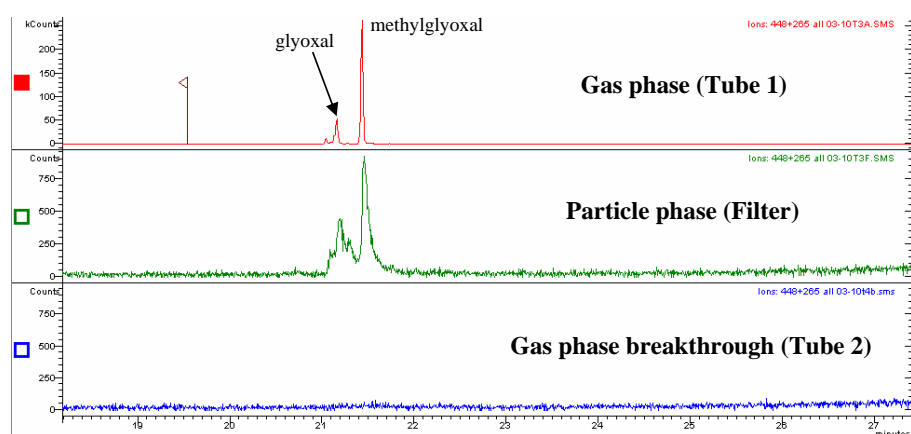


Fig. 6. Reconstructed ion chromatograms ($m/z=448+265$) comparing the relative gas-phase, particle-phase and gas-phase breakthrough concentrations of glyoxal and methylglyoxal for experiment ISO_PSI_1. The particle-phase and gas-phase breakthrough chromatograms are on the same scale.

4762

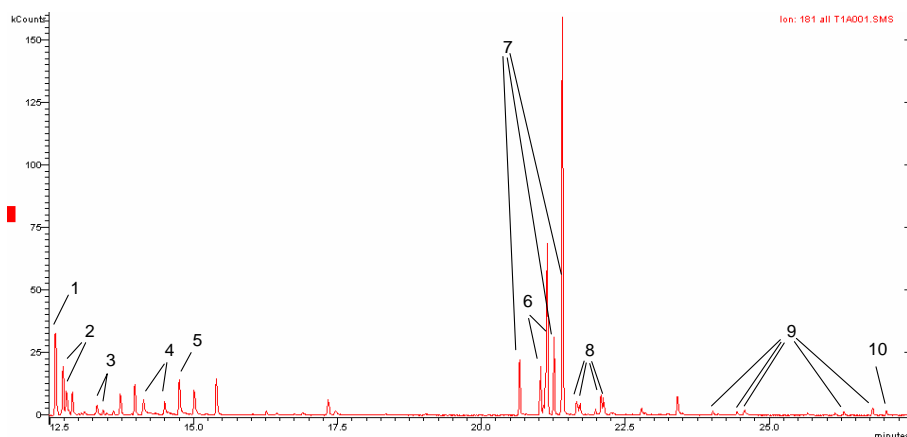


Fig. 7. Reconstructed ion chromatogram (m/z 181) of a denuder extract from the photooxidation of isoprene (experiment ISO_UCC_1). 1: methacrolein 2: methylvinylketone 3: 2-methylbut-3-enal 4: glycolaldehyde 5: hydroxyacetone 6: glyoxal 7: methylglyoxal 8: oxopropanedial 9: methylbutenedial 10: butenedial.

4763

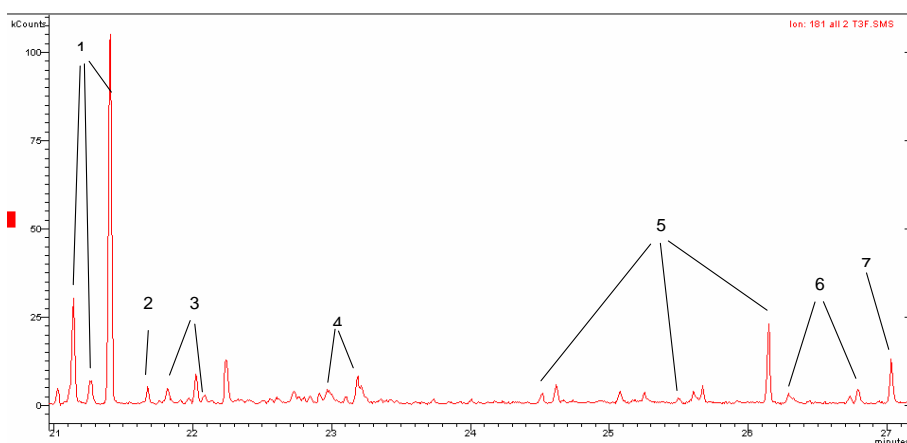


Fig. 8. Reconstructed ion chromatogram (m/z 181) of a filter extract from the photooxidation of 1,3,5-TMB (experiment TMB_UCC_2). 1: methylglyoxal 2: oxopropanedial 3: 2,3-dioxobutanal 4: 3-hydroxy-2,4-pentanedione 5: 2-methyl-4-oxo-2-pentenal 6: 2-methylbutenedial 7: butenedial.

4764